Journal of Applied Fluid Mechanics, Vol. 14, No. 2, pp. 541-553, 2021.
Available online at www.jafmonline.net, ISSN 1735-3572, EISSN 1735-3645.
DOI: 10.47176/jafm.14.02.31778

Uncertainty Analysis of Experiments of Vortex-Induced Vibrations for Circular Cylinders

O. Usta[1†] and A. Duranay[2]

[1] *Department of Naval Architecture and Marine Engineering, Turkish Naval Academy, National Defence University, 34942, Tuzla – Istanbul – Turkey*
[2] *Faculty of Naval Architecture and Ocean Engineering, Istanbul Technical University, Istanbul, 34467, Turkey*

†Corresponding Author Email: ousta@dho.edu.tr

(Received May 3, 2020; accepted August 27, 2020)

ABSTRACT

In this study, uncertainty analysis of the vortex-induced vibration (VIV) tests, using a VIV test rig is presented. The VIV test rig is set up on the circulation channel in Ata Nutku Ship Model Testing Laboratory at Istanbul Technical University (ITU). The tests are performed using an elastically mounted rigid and smooth circular cylinder in low mass-damping and high Reynolds numbers conditions. The cylinder has one-degree-of freedom. It is allowed to move perpendicular to the flow while inline vibrations are constrained. The aim of the study is to demonstrate and establish a repeatable procedure to predict the uncertainty of VIV tests, utilizing some example applications of existing ITTC recommendations. Within this aim, five distinct VIV tests are carried out following ITTC guidelines and procedures measuring the amplitude (A^*) and frequency response (f^*) data. Uncertainty analysis study is performed for three different flow velocities, chosen from VIV tests and total uncertainty is calculated by root mean square values of precision and bias uncertainties. The precision uncertainty is predicted using response amplitude values obtained from five sets of VIV tests. The bias uncertainty is predicted utilizing the basic measurements and test results of the components of response amplitude for the cylinder. The results have demonstrated that the current test rig has low uncertainty level. Additionally, it has succeeded to reflect the characteristics of VIV phenomenon in the studied Reynolds number range, which is in the Transition Shear Layer 3 (TrSL3) flow regime. Consequently, it is believed that this study would help in spreading the application of the uncertainty analysis for VIV tests in the future.

Keywords: Vortex-induced vibration; VIV; Uncertainty analysis; Bias error; Precision error; Response amplitude.

NOMENCLATURE

A	amplitude of oscillation
A^*	response amplitude of cylinder
B_{total}	total bias uncertainty
B_{A^*}	bias error of response amplitude
B_{C_y}	bias error of lift coefficient
B_{m^*}	bias error of mass ratio
$B_{m^*\zeta}$	bias error of mass-damping parameter
B_{f^*}	bias error of frequency ration
B_{U^*}	bias error of reduced velocity
B_{Φ}	bias error of phase angle
C_A	added mass coefficient
C_P	pressure coefficient
C_x	lift coefficient (x direction)
C_y	lift coefficient (y direction)
D	cylinder diameter
f	frequency of oscillation
$f_{n,w}$	natural frequency in water
f^*	frequency ratio
F	hydrodynamic force
L	cylinder length
k	stiffness
m	mass
m_{disp}	displacement mass
m^*	mass ratio
N	number of independent observations
P_{total}	total precision uncertainty
P_{A^*}	precision error of response amplitude
$\bar{q}$	the mean or average value
Re	Reynolds number
S	standard deviation
$u(\bar{q})$	standard uncertainty for the average value
$u_c(y)$	combined uncertainty
u_{ex}	extended uncertainty
U	flow velocity
U^*	reduced flow velocity
U_{total}	total uncertainty

ζ Damping ratio

1. INTRODUCTION

Vortex induced vibrations (VIV) are motions induced on bluff bodies which get excited by an external fluid flow. Bluff marine structural bodies generally consisting of cylindrical components, such as offshore platforms, pipelines and risers that can experience vortex shedding in currents. Vortex shedding process induces periodic forces on the body which can generate vibrations in axial (in-line vibration, shortly IL) and transversal (cross-flow vibration, shortly CF) directions (ITTC Report No 7.5-02-07-03.10, 2014). This fluid-structure interaction, VIV, has been extensively investigated during the recent years by virtue of its considerable effects on various engineering structures such as bridges, skyscrapers, towers, power transmission lines and offshore structures (Modir and Goudarzi, 2019). Thus, it can be stated that the study of VIV consists of a number of disciplines that incorporate fluid/structural mechanics vibrations/acoustics and computational fluid dynamics (Williamson and Govardhan, 2006).

VIV is generally known for its destructive effects on engineering structures. However, research in recent years has shown that it is possible to develop engineering mechanisms by taking advantage of VIV and put them into beneficial uses (Bernitsas *et al.* 2008; Modir and Goudarzi, 2019). For example, it is possible to generate renewable energy with the VIV arrangement placed in a stream, or a similar device to be placed in the same stream can be driven by a device such as a pump.

Literature review indicates that VIV motions have unstable characteristics and various flow regimes. Several critical dimensions of the phenomenon have yet to be clarified, and questions have yet to be answered relating to the dominant response frequency, phase angle variation (i.e., according to which the force results in displacement), and normalized velocity range. Another important consideration is the response amplitude in the synchronization range, which serves as a function of the influencing and governing parameters. In the case of industrial applications, these continue to draw attention to the challenges associated with forecasting the dynamic response of interactions that occur between structures and fluids. More research is required for the investigation of the force coefficients, damping coefficients, correlation lengths, relative roughness, waves, shear, and currents and other governing and influencing parameters. Significant safety-related factors are also relevant to consider. It is expected that, considering the publication of results from studies with large examples, the literature will keep advancing on questioning the connections between a structure's response and the influencing and governing parameters (Carberry, 2001; Sarpkaya, 2004; Sumer and Fredsoe, 2006; Williamson and Govardhan, 2006; Bernitsas *et al*. 2008; Lee and Bernitsas, 2011; Kinaci *et al*. 2016a; Modir and Goudarzi, 2019). Thus, these parameters should be considered determining the uncertainty of VIV tests.

Computational fluid dynamics based methods are relatively new in this field. Wu *et al*. (2014), Kinaci (2016) and Dobrucali and Kinaci (2017) performed numerical analysis study to evaluate the flow induced motion of circular cylinder for different conditions, using URANS model and compared them with VIV experiments. Kinaci *et al*. (2016b) assessed the turbulence effect on the flow induced motion of a circular cylinder, comparing numerical and experimental results. Zhang *et al*. (2017) investigated the energy that obtained by using bluff bodies working in different cross sections. Pigazzini *et al*. (2018) investigated VIV motion of an elastically mounted 2D cylinder by using a single degree of freedom, multi frequency code. Grioni *et al*. (2020) conducted a computational study to investigate the flow interference between two circular cylinders in tandem by the scale-adaptive simulation technique.

Vortex-induced vibrations of cylinders have been investigated experimentally for years; hence, there is significant literature on this phenomenon. Many researchers in different laboratories conduct experiments to generate new information. Gopalkrishnan (1993), conducted VIV experiments of oscillating cylinders to examine the forces generated by VIV motions. Khalak and Williamson (1999) analyzed the mode transitions and generated forces in VIV, in low mass damping condition. Williamson and Govardhan, (2004 and 2006), Sarpkaya (2004), Sumer and Fredsoe (2006), carried out VIV experiments to get more insight into the details of VIV phenomenon. Klamo *et al*. (2005) conducted VIV experiments to investigate the maximum amplitude of a freely vibrating cylinder and Modir *et al*. (2016) investigated the effect of mass ratio, while Modir and Goudarzi (2019) investigated the effect of spring stiffness and Reynolds number on vortex induced vibrations of cylinder. In the study of Modir *et al*. (2016), flexibly mounted cylinder is used, however, Modir and Goudarzi (2019) used rigid cylinder. Bernitsas *et al.* (2008), developed a device called VIVACE and conducted VIV tests to investigate its performance, and Lee and Bernitsas (2011), used this VIVACE converter to obtain renewable energy. Arshad *et al.* (2018) investigated the effect of fin geometry on VIV response. They especially focused on fin thickness and fin density. Mumtaz Qadri *et al*. (2019) carried out an experimental study to investigate energy harvesting performance of passively flapping motions.

Literature review study showed that, even though physical formation and mathematical modelling of

the VIV tests have been investigated extensively, the methods to predict the uncertainty for VIV tests are not clearly explained and standardized. In addition, in the last published ITTC (International Towing Tank Conference) guideline for VIV testing (ITTC, Report No 7.5-02-07-03.10, 2014) and the ITTC report (Qiu, 2014), it is stated that, uncertainty analysis should be performed for VIV experiments, in accordance with the ITTC procedures. Thus, in this study, uncertainty analysis for VIV tests of a cylinder has been carried out by utilizing various ITTC reports, guidelines and procedures (ITTC, Report No 7.5-02-02-02, 2002; ITTC, Report No 7.5-02-01-01, 2014; ITTC, Report No 7.5-02-03-01.2, 2017). To the authors' knowledge, an uncertainty analysis to predict the uncertainty components of bias and precision are carried out for the first time in the literature within this study.

Within the above context, the main purpose of the study is to establish and propose a reliable and repeatable procedure to predict the uncertainty of VIV tests using a rigid and smooth circular cylinder on elastic springs, at low mass damping and high Reynolds number conditions. This aim is attempted by conducting five distinct VIV tests and calculating the uncertainty for three different flow velocities, utilizing some example procedures proposed by the ITTC (ITTC, Report No 7.5-02-07-03.10, 2014). It is believed that, this study would help in spreading of the application of uncertainty analyses for VIV tests.

In order to satisfy the above aim, this study is organized accordingly. Following this introduction, Section 2 presents uncertainty analysis in engineering measurements demonstrating the existing the procedures for uncertainty analysis mostly published by the ITTC. Section 3 describes the experimental facilities and test conditions. In Section 4, uncertainty analysis procedure for the VIV tests that is proposed is detailed and discussed. Finally, the overall conclusions obtained from this study are presented in Section 5.

2. UNCERTAINTY ANALYSIS IN EXPERIMENTAL HYDRODYNAMICS

Experiments are carried out within the almost identical conditions to the theoretically determined conditions. If the experimental results and theoretical results of any investigated parameter are compared, even if the conditions are the same as far as we know, there is a difference. The difference between the theoretical value and experimentally obtained (measured) value is defined as error, and the prediction of this error is called as uncertainty (Insel, 2008).

Uncertainty of a measurement is a parameter that could be attributed to the measurand. An ideal expression of the uncertainty of a measurement is universal and transferrable to other problems in engineering (JCGM 100:2008, 2008). According to ITTC (ITTC, Report No 7.5-02-01-01, 2014), results of an uncertainty assessment should not just present an estimated range of the total uncertainty. It should also include accurate reporting of uncertainty parameters and explanations of the methods used in the evaluation of the uncertainty components.

All measured data, in hydrodynamic experiments, contain a certain degree of uncertainty. Even if the tests carried out in constant conditions, test results may be different from each other because of various uncertainty components. Hence, the extent to which the experimental results can be relied upon is understood from conducting a proper uncertainty analysis (Delen and Bal, 2015; Bunt *et al*. 2019).

Theory of the uncertainty analysis is described in detail by various organizations such as American Society of Mechanical Engineers (ASME), International Organization for Standardization (ISO) and American Institute of Aeronautics and Astronautics (AIAA). They have contributed in recommending procedures for uncertainty analysis for different engineering disciplines.

Currently, ITTC (International Towing Tank Conference) has two procedures to conduct uncertainty analyses in experimental hydrodynamics. One was generated according to the procedures of ASME (ASME, 2005), and the other was generated according to the ISO (ISO, 2008).

In the rest of this study, these two methods are shortly called as the ASME method that is used by (ITTC, Report No 7.5-02-02-02, 2002; Insel, 2008; ITTC Report No 7.5-02-03-01.2, 2017) and the ISO method used by (ITTC, Report No 7.5-02-02-02, 2014; Qui *et al*. 2014; Bunt *et al*. 2019).

2.1 Uncertainty Evaluation by ISO Method

In ISO method, components that generate uncertainty are divided into two parts. The one that is called Type A is calculated by utilizing statistical analysis of (many) repeated measurements, while the other one, Type B is calculated by using all relevant information that is available on the measurement process, including past experience (Qiu *et al*. 2014; Bunt *et al*. 2019). Both types of evaluation are based on probability distribution. ISO divides the uncertainty into three groups:

- standard uncertainty u,
- combined uncertainty $u_c(y)$,
- extended uncertainty u_{ex}

Standard uncertainty of a measurement can be calculated by using standard deviation (ISO, 2008). In calculation of Type A uncertainty, statistical analysis of a series of observations are used. The average value of the obtained tests results are calculated by using Eq. 1.

$$\bar{q} = \frac{1}{N} \sum_{k=1}^{N} q_k \tag{1}$$

Where, N is the number of independent observations and q_k is a measured quantity for kth observation.

Equation 2 and Eq. 3 can be used to calculate standard deviation of q_k and the average value of the standard uncertainty.

$$s^2 = \frac{1}{N-1}\sum_{k=1}^{N}(q_k - \bar{q})^2 \quad (2)$$

$$u(\bar{q}) = \frac{s}{\sqrt{N}} \quad (3)$$

To calculate the Type B uncertainty, it is needed to have hand-book information, general knowledge, past experience, pre-test measurements, and manufacturer specifications for the investigated parameter (Park *et al*. 2015).

Combined uncertainty is a standard uncertainty, that takes into account contributions from all considerable uncertainty sources by combining the respective uncertainty components (ISO, 2008).

Extended uncertainty can be obtained by multiplying the combined standard uncertainty by a standard coefficient. Thus, a specified level of confidence can be given to the uncertainty (ISO, 2008). Extended uncertainty can be calculated by the Eq. 4.

$$u_{ex} = k * u_c(y) \quad (4)$$

where, k is the mentioned coefficient, also known as coverage factor.

Extended uncertainty reflects the level of confidence that the estimate of the measurand is within an interval of $\pm U$ around the best estimate of the measurand. In experimental hydrodynamic model testing, a confidence level of 95% is justified (ITTC, Report No 7.5-02-02-02, 2002). In that case, the coverage factor k is equal to 2 (ISO, 2008).

For wider explanation and mathematical background of the ISO method, reference (Qiu *et al*. 2014) could be referred to.

2.2 Uncertainty Evaluation by ASME Method

ASME is divided the components that generate uncertainty into two groups. One is the bias uncertainty and the other is the precision uncertainty. By calculating the root mean squares of these two, the total uncertainty is determined. The precision uncertainty is calculated by a method depends on standard deviation and is consists of the errors of measured data. The bias is a systematic uncertainty source, can be calculated by considering the effects separately or combination of effects. Basic measurements that depends on general knowledge, past experience, pre-test measurements etc. and the effect of test results that can be calculated by the mathematical expressions derived for the investigated parameter are the main sources of bias uncertainty (ITTC, Report No 7.5-02-03-01.2, 2017).

We repeat the experiments many times and try to generate the same conditions in our experiments to obtain reliable and repeatable results. However, we cannot generate exactly the same conditions in each repetitive tests. We can only generate almost the same conditions. Precision uncertainty depends on statistical fluctuations in the measured data of repetitive tests. Thus, it is related to the number of experiments and it is evaluated via repeated measurements. The more we repeat the tests as much as possible under the same conditions, the smaller the precision uncertainty. However, the bias uncertainties may be assumed constant for a specified experimental parameter (ITTC, Report No 7.5-02-03-01.2, 2017).

In ASME method, total uncertainty is calculated by using bias and precision uncertainties, as given by Eq. 5.

$$U_{total} = \sqrt{(B_{total})^2 + (P_{total})^2} \quad (5)$$

where B_{total} is total bias uncertainty, P_{total} is total precision uncertainty and U_{total} is total uncertainty.

Bias uncertainty can be obtained by calculating the square root of the sum of the squares of the bias components (ITTC, Report No 7.5-02-02-02, 2002).

$$B_{total} = \sqrt{(B_a)^2 + (B_b)^2 + \cdots (B_N)^2} \quad (6)$$

where B_a and B_b represents the bias components and N is the number of bias uncertainty components.

Uncertainty analysis by using ASME method is detailed in Section 4.

2.3 Selection of the Uncertainty Evaluation Method for VIV Tests

As detailed in the previous sub-sections, ASME method and ISO method are two different approaches to estimate the uncertainty on measured results for experimental hydrodynamics studies. Even though the mathematical background of these methods are different, the main theme of them are quite similar and they do not contradict with each other (Delen and Bal, 2015).

The ASME method considers the predictions of the effects of a great number of examinable uncertainty sources on the results. It depends on taking the account of each component, as much as possible. However, the ISO method investigates the dominant components that have impact on the measured results (Delen and Bal, 2015).

Physics behind the VIV is very complicated and there are many components effecting the result in VIV equation (response amplitude equation A^*), given Eq. 7). For this reason, it is very difficult to know which components are more dominant, how they are affecting the results and how they should be compared. Thus, according to the authors' knowledge perspective on the subject, each parameter should take into account in the uncertainty analysis.

The main purpose in this paper is to reach the most accurate results in uncertainty analysis by combining up-to-date academic knowledge and engineering perspective. Within this context, it is believed that, using the ASME method for uncertainty evaluation in VIV tests will provide more accurate results, than ISO method. Thus, uncertainty analysis calculations have been conducted according to the ASME method, examined and exemplified by the ITTC (ITTC, Report No 7.5-02-02-02, 2002; ITTC Report No 7.5-02-03-01.2, 2017).

3. EXPERIMENTAL FACILITIES AND TEST CONDITIONS

VIV experiments have been carried out on the channel located in the Ata Nutku Ship Model Testing Laboratory at ITU. The circulation channel is 1.5 meters wide, 0.64 meters deep. Although the channel was built in 1970s, it has been renovated in 2019, including its digital controllers, before the VIV apparatus was installed. Ata Nutku Circulation Channel is shown in Fig. 1.

Fig. 1. Ata Nutku Circulation Channel.

Some experiments have been conducted to test the capabilities of the setup before this study and will soon be published in (Duranay and Kinaci, 2020). The channel streams a uniform steady current over a range of $0 < U < 1.56 m/s$ towards the VIV apparatus while the apparatus is stationary.

The VIV test rig consists of a shaft, two elastic springs, holders, a circular cylinder, two struts and measurement devices. The cylinder extends to both sides of the test section as much as possible to avoid downwash that might lead to loss of flow from the tips (Kinaci *et al*. 2016a). The ratio between the distance of channel walls as well as the length of the rigid circular cylinder is 0.88 and the blockage ratio is %12.5. ITTC's recommended procedures and guidelines for VIV testing are followed for while selecting each component of the system (ITTC, Report No 7.5-02-07-03.10, 2014).

Fig. 2. The VIV test rig used is the tests.

For the performance assessment of the test rig, five distinct tests are conducted using same parameters, given in Table 1.

Table 1 VIV Test Rig particulars

Parameter	Value or Range
Cylinder Diameter (mm)	80
Cylinder Length (mm)	1320
Spring stiffness (N/m)	375
Mass ratio	2.34
Velocity ratio	3.90-15.00
Reynolds number	20.000-63.000
Damping ratio	0.0614

Seen from Fig. 3 and Fig. 4, the results of five distinct tests are quite similar especially in the initial and upper branches, which is to be expected for a system having low uncertainty value. Each measurement is recorded 60 seconds and the average values are calculated from the peaks of oscillations.

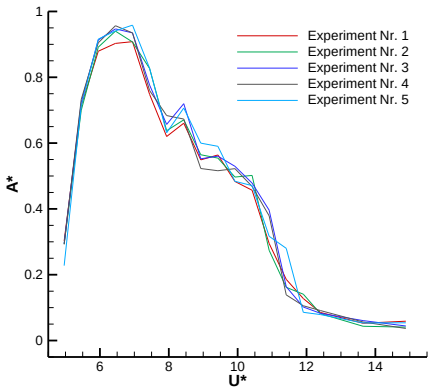

Fig. 3. Amplitude responses of the cylinder in five different runs.

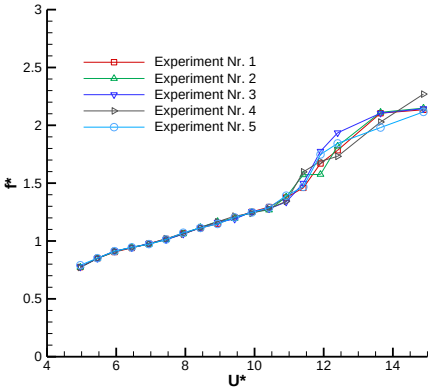

Fig. 4. Frequency responses of the cylinder in five different runs.

As in terms of the frequency response, it increases almost linearly with increasing reduced velocity. VIV motion achieves higher frequencies creating irregular span-wise vibrations that ends up with less analogous measurement results. Therefore, tests diverge from each other at lower branch region

where frequency of oscillation is comparatively higher. These test results show that three distinct branches at these Reynolds numbers defined by (Raghavan and Bernitsas, 2011) can be observed.

4. UNCERTAINTY ANALYSIS OF VIV TESTS

In this section, the uncertainty analysis for the five distinct VIV tests are carried out for three different flow velocities. Uncertainty analyses are carried out following the procedures of ITTC (ITTC, Report No 7.5-02-02-02, 2002; ITTC Report No 7.5-02-03-01.2, 2017), which depends on ASME method (ASME, 1999).

Uncertainty assessments are conducted utilizing the basic measurements and experimental results of the components of the response amplitude equation (A^*), given by Eq. 7. Bias and precision uncertainties are predicted separately for the test results of response amplitude values of the cylinder in water. A procedure for the calculation of the uncertainty in VIV tests is proposed. The aim of the proposed procedure is to provide an example work to predict the uncertainty for the VIV measurements.

The parameters causing uncertainties for VIV tests can be categorized as initial conditions such as properties of the fluid, model characteristics (geometry), environmental conditions, scaling effect, used apparatus (electronic devices etc.) and human factor. The amplitude of a cylinder in VIV tests, however, mainly depends on the components that given in Eq. 7, such as the magnitude of the force coefficients, mass ratio (the relative mass of the body to the displaced water mass), flow velocity (reduced velocity), structural damping and the parameters related frequency of vibration (ITTC, Report No 7.5-02-07-03.10, 2014).

According to the ITTC guidelines referred, the tests should be repeated for five sets, in order to achieve reliable precision uncertainty. In this paper, ITTC recommendations are considered and VIV tests are carried out 5 sets for 3 different flow velocities (0.338, 0.390 and 0.442 m/s which values correspond with upper and lower branches) measuring the response amplitude (A^*) and frequency (f^*) data, for each velocity giving 5 test points, 15 test points in total.

4.1 Mathematical Background of the Uncertainty Analysis for VIV Measurements

When an uncertainty analysis is carried out for a real case, the details should be tailored to the each equipment used and the test procedures followed (ITTC, Report No 7.5-02-02-02 2014). Although a recent study defines VIV using oscillation frequency (Bernitsas *et al*. 2019), uncertainty analysis calculations in this study are conducted using the components of the response amplitude equation (A^*). This is because the response amplitude equation composed of various components affecting the characteristics of the VIV motion, including the frequency ratio as well.

$$A^* = \frac{1}{4\pi^3}\frac{C_y \sin\Phi}{(m^*+C_A)\zeta}\left(\frac{U^*}{f^*}\right)^2 f^* \tag{7}$$

In this equation, C_y is the lift coefficient in y direction, Φ is the phase difference between fluid force and displacement, m^* is the mass ratio, C_A is potential added mass coefficient, ζ is the damping ratio, U^* is the reduced velocity factor and f^* is the reduced frequency.

The precision uncertainty of the response amplitude measurements is predicted using test results of the response amplitude (A^*) and frequency (f^*) values of five sets flow velocities.

The bias uncertainty of the measured response amplitude is composed of two steps: the first step is the bias uncertainty predictions of the basic measurements such as model length, model diameter, displacement, density of water, temperature of water, flow velocity and viscosity of water. In the second stage, bias uncertainty results obtained in the first stage are used. The second step is calculating the bias uncertainties of the components of Eq. 7 such as lift coefficient, mass displacement, added mass coefficient, mass-damping parameter, frequency ratio, reduced velocity and the phase angle. Total bias uncertainty is calculated by the root mean squares of the bias uncertainties of these components.

As a result, the uncertainty for the response amplitude (A^*) can be calculated by using bias and precision uncertainties as given by Eq. 8.

$$U_{A^*} = \sqrt{(B_{A^*})^2 + (P_{A^*})^2} \tag{8}$$

In the study, bias uncertainty predictions for the response amplitude is divided into two main parts, such as bias uncertainty of basic measurements and bias uncertainty of the components that exist in response amplitude equation, separately. Bias uncertainty of basic measurements are calculated following ITTC guidelines and obtained test results. Then the bias uncertainty of the components that exist in response amplitude equation are calculated using the partial derivatives of each components that exist in their own mathematical formulations, utilizing the bias uncertainty of basic measurements. The precision uncertainty is calculated using the data obtained from VIV measurements.

4.2 Precision Uncertainty Predictions

The precision uncertainty for the for the response amplitude (A^*) are estimated by end-to-end method given in ITTC procedures using the measured data of response amplitude (A^*) and frequency (f^*). (ITTC, Report No 7.5-02-02-02, 2002; ITTC Report No 7.5-02-03-01.2, 2017).

ITTC recommends that, when the model removed and reinstalled again, standard deviation should be determined for each set of measurements. (ITTC, Report No 7.5-02-02-02, 2002). While calculating the precision error, test results of response amplitude (A^*) and frequency (f^*) data for 5 sets of VIV tests in the flow velocities of U= 0.338 m/s presented in Table 2 are used.

Table 2 Precision uncertainty data for U=0.338 m/s

Test No	Measured Values		
	A^*	f^*	C_y
1	0.9028	0.9402	0.5184
2	0.9401	0.9472	0.5438
3	0.9469	0.9418	0.5447
4	0.9565	0.9429	0.5508
5	0.9410	0.9456	0.5432
Mean	0.9375		0.5402
Sdev			0.0112

As a result, of five repetitions of the experiments, mean values and standard deviations are calculated. Then the precision uncertainty for the tests can be calculated as:

$$P_{A^*} = \frac{k\,SDev}{\sqrt{M}} \tag{9}$$

where M is the number of tests that is repeated, $SDev$ is the standard deviation. k represents the coverage factor and it is assumed that K=2 with the ITTC (ITTC Report No 7.5-02-03-01.2, 2017) reference.

$$P_{A^*} = \frac{2*0.0112}{\sqrt{5}} = 0.0224 \tag{10}$$

Thus, the total precision uncertainty for the VIV tests is calculated as P_{A^*}= 0.0224. This error corresponds to the 2.393 % of the mean A^* value of 0.9375.

4.3 Bias Uncertainty Predictions

Bias uncertainty predictions for the response amplitude can be divided into two main parts such as bias uncertainties of basic measurements and bias uncertainties of the components that exist in response amplitude equation.

4.3.1 Basic Measurements

Basic measurements, which generate uncertainty, can be sorted as model length, model diameter, displacement, density of water, temperature of water, flow velocity and viscosity of water. The bias uncertainties of these parameters are calculated separately following the procedures and guidelines published by ITTC (ITTC, Report No 7.5-02-02-02, 2002; ITTC, Report No 7.5-01-01-01, 2002; ITTC Report No 7.5-02-03-01.2, 2017).

4.3.1.1 Cylinder Geometry

Manufacturing process cannot be completely error free and therefore the geometry of the cylinder used in the tests has error. The influence of the error in cylinder form affects the flow characteristics around the cylinder and hence generated uncertainty in the test results. Although there can be different error sources in cylinder geometry; cylinder length, cylinder diameter as well as projected area are considered to be the main geometrical sources to generate bias error in this study.

Cylinder length L: ITTC recommends that the uncertainty in model geometry length can be adopted as ±1 mm in all coordinates (ITTC, Report No 7.5-01-01-01, 2002). Hence the bias uncertainty in cylinder length can be assumed as B_L =2 mm (B_L=0.002).

Cylinder diameter D: Similar to cylinder length, bias uncertainty in cylinder diameter is assumed as D=2 mm (B_D=0.002).

4.3.1.2 The displacement mass ($\mathbf{m_{disp}}$)

The balance in our laboratory is calibrated to ± 1.0 kg, following the calibration process for the model weight measurements given by ITTC (ITTC, Report No 7.5-02-02-02, 2002). Accordingly, the weight of the cylinder with the equipment is measured.

The displacement mass (m_{disp}) of the model is calculated as:

$$m_{disp} = \rho\pi\left(\frac{D}{2}\right)^2 L = 0.635 \text{ kg} \tag{11}$$

If the dimensions are changed as given section 4.3.1.1, the displacement mass is calculated as;

$$m_{disp}{}' = 6.981 \text{ kg} \qquad \Delta m = 0.3464 \text{ kg} \tag{12}$$

4.3.1.3 Flow Velocity *U*

Flow velocity system consists of individual measurement systems. A digital revolutions per minute (rpm) controller is used to scale the velocity of current, over a range 0<U<1.56 m/s. The circulation channel mainly consists of a control panel and main engine. A calibration for the circulation mechanism was carried out using a digital flow speed meter. Figure 5 shows the calibrated values for the circulation velocities. Here n and V are mean rpm and velocity respectively. Based on the results acquired from the calibration tests, a calibration factor of 0.0013 is multiplied to rpm values to determine the corresponding current velocity.

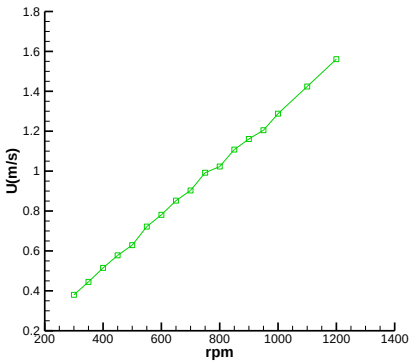

Fig. 5. Circulation Channel Calibration.

Bias uncertainty calculations of the flow velocity is followed from ITTC procedure (ITTC, Report No 7.5-02-02-02, 2002). A correlation is set between the carriage speed measurement system of a towing tank and flow velocity measurement system used in the VIV tests. Bias error of flow velocity is calculated as $B_U = 0.0036$ m/s. (The bias uncertainty for the blockage effects is neglected).

Bias uncertainty for flow velocity $B_U = 0.0036$ m/s equals to 1.057% uncertainty, that of U=0.338 m/s.

4.3.1.4 Water Temperature

Since the accuracy of thermometer in our laboratory is ±0.5 degrees, the bias uncertainty associated with the temperature measurement is adopted as B_{t^o}=0.5 degree, following the ITTC guideline (ITTC, Report No, 7.5-02 01-03, 1999).

4.3.1.5 Water Density

The density-temperature relationship can be calculated according to the ITTC (ITTC, Report No, 7.5-02 01-03, 1999).

$$\rho = 1000.1 + 0.552\,t^o - 0.0077\,t^{o^2} + 0.00004\,t^{o^3} \quad (13)$$

$$\frac{\partial \rho}{\partial t} = \left|0.055 - 0.0154\,t^o + 0.00012\,t^{o^2}\right| = 0.1488 \quad (14)$$

$$B_{\rho 1} = \frac{\partial \rho}{\partial t^o} B_{t^o} = 0.04464 \quad (15)$$

$B_{\rho 2}$ is the error resulting from the compliance of the data with the curve when calculating the density-dependent equation of the temperature. It can be calculated by two times of standard error estimate (*SEE*). *SEE* is predicted as 0.035 using the data given in (ITTC, Report No 7.5-01-01-01, 2002).

$$B_{\rho 2} = 2*SEE\ 2*0.035 = 0.070\ \text{kg/m}^3 \quad (16)$$

$B_{\rho 3}$ is caused by the difference between the water density depending on the temperature of the water found in the equation and the water density used in the calculations.

$$B_{\rho 3} = 1000 - 999.3305 = 0.669\ \text{kg/m}^3 \quad (17)$$

$$B_\rho = \sqrt{\left(B_{\rho 1}\right)^2 + \left(B_{\rho 2}\right)^2 + \left(B_{\rho 3}\right)^2} = 0.674\ \text{kg/m}^3 \quad (18)$$

In conclusion, the bias uncertainty for density is calculated as 0.6746 kg/m^3, equals to 0.674 % of ρ = 1000 kg/m^3

4.3.1.6 Kinematic Viscosity

Uncertainty of the kinematic viscosity is adopted by ITTC (ITTC, Report No, 7.5-02 01-03, 1999) can be calculated using Eq. 19.

$$\nu = (0.585*10^{-3}(t\text{-}12) - 0.00336)*(t\text{-}12) + 1.235)*10^{-6} \quad (19)$$

Depending on the water temperature t=15 ^oC and $B_t = 0.3$; B_{v1} is calculated using Eq. 20.

$$B_{v1} = \left|\frac{\partial \nu}{\partial t^0}\right| B_{t^0} = 9.030*10^{-9}\ \text{m/s}^2 \quad (20)$$

Kinematic viscosity is obtained from ITTC guideline (ITTC, Report No, 7.5-02 01-03, 1999), which is ν =1.13902*10^{-6}m/s^2. Using this information, the bias uncertainty corresponding from the difference between test and ITTC report is;

$$B_{v2} = -4.15*10^{-10}\ \text{m/s}^2 \quad (21)$$

In conclusion, the total bias uncertainty is calculated:

$$B_v = \sqrt{(B_{v1})^2 + (B_{v2})^2} = 9.0395*10^{-9}\ \text{m/s}^2 \quad (22)$$

This uncertainty corresponds to 0.793% of the kinematic viscosity ν=1.139*10^{-6} m/s^2.

4.3.2 Bias Uncertainty Predictions for the Components That Exist in Equation A^*

The following sub-sections (4.3.2.1 – 4.3.2.7) covering the bias uncertainty predictions for U=0.338 m/s.

4.3.2.1 Lift Coefficient (C_y)

The power of a VIV cylinder that comes from water is related to the lift coefficient, C_y (Williamson and Govardhan, 2006). The lift coefficient (C_y) is function of lift force, length and diameter of the cylinder, velocity of the flow and density of water in the water tank given in Eq. 23.

$$C_y = \frac{F_y}{\frac{1}{2}\rho\, U^2\, D\, L} \quad (23)$$

where; F_y is the the force exerted by the fluid on the body in the y-direction. Thus, the bias uncertainty of the lift coefficient (C_y) can be calculated using the Eq. 24, if the lift force measurements were performed experimentally. In this study, however, the lift coefficient values are obtained from CFD analysis. For this reason, the bias uncertainty for the lift coefficient is estimated considering CFD procedures. The numerical uncertainty in CFD analysis can be predicted based on the Grid Convergence Index (GCI), which is composed of grid and time step errors. Examining the studies performed by Tezdogan *et al*. (2015) and Usta and Korkut (2018), the numerical uncertainty for grid and time-step is estimated as 4%, for grid and time step seperately. The lift force obtained from VIV tests was $C_y = 0.10396$. Hence, 4 % of the lift coefficient gives the bias uncertainties of grid and time-step as presented Eq. 25 and total bias uncertainty of lift coefficient is given by Eq. 26.

$$B_{C_y} = \sqrt{\left(\frac{\partial C_y}{\partial L} B_L\right)^2 + \left(\frac{\partial C_y}{\partial D} B_D\right)^2 + \left(\frac{\partial C_y}{\partial U} B_U\right)^2 + \left(\frac{\partial C_y}{\partial \rho} B_\rho\right)^2 + \left(\frac{\partial C_y}{\partial F_y} B_{F_y}\right)^2} \quad (24)$$

$$B_{C_{y_{grid}}} = 0.00416, \quad B_{C_{y_{time-step}}} = 0.00416 \quad (25)$$

$$B_{C_{y_{CFD}}} = \sqrt{\left(B_{C_{y_{grid}}}\right)^2 + \left(B_{C_{y_{time-step}}}\right)^2} = 0.0588 \quad (26)$$

In accordance, total bias uncertainty of the lift coefficient is predicted as B_{C_y} =0.0588.

4.3.2.2 Mass Ratio (m^*)

According to the Bernitsas *et al*. (2008), the mass

ratio of a VIV can be expressed as the total oscillating mass of the cylinder, including all oscillating appendages and 1/3 of the spring mass, divided by the displaced fluid mass m_d.

$$m^* = \frac{m_{osc}}{m_{disp}} = \frac{m_{osc}}{\pi/4\,\rho\, D^2\, L} \tag{27}$$

where m_{osc} is the oscillating mass and m_{disp} is the mass displacement of the cylinder (weight of the cylinder).

In our test rig, the weight of the overall oscillating mechanism is 15.5 kg, the weight of the cylinder is 6.635 kg. Thus, the mass ratio of the cylinder m^*equals to 2.336.

Sensitivity of the weighting instrument that is used to weigh the oscillating mechanism is ± 50 gr. For this reason, bias error for oscillating mass $B_{m_{osc}}$ is assumed to be is $B_{m_{osc}} = 0.05$.

Corresponding the Eq. 27, the bias uncertainty for the mass ratio (m^*) can be calculated for density of water, diameter and length of cylinder and oscillating mass, as given in Eq. 28 below.

The total bias uncertainty of the mass ratio (m^*), calculated according to Eq. 28 is B_{m^*} =0.00847.

$$B_{m^*} = \left(\frac{\partial m^*}{\partial L} B_L\right)^2 + \left(\frac{\partial m^*}{\partial D} B_D\right)^2 + \left(\frac{\partial m^*}{\partial \rho} B_\rho\right)^2 + \left(\frac{\partial m^*}{\partial m_{osc}} B_{m_{osc}}\right)^2 \tag{28}$$

4.3.2.3 Mass-Damping Parameter ($m^*\zeta$)

In the studies of Williamson and Govardhan (2004; 2006) and Sarpkaya (2004), it is explained that the $m^*\zeta$ that is called as mass-damping parameter controls the maximum amplitude of the oscillation. For this reason, the bias uncertainty of $m^*\zeta$ is predicted and used as one of the bias error components in A^* (Eq. 7), in this study. The bias error for the mass-damping parameter ($m^*\zeta$) can be calculated using Eq. 29.

$$B_{m^*\zeta} = \sqrt{{B_{m^*}}^2 + {B_\zeta}^2} \tag{29}$$

The total bias uncertainty for the mass-damping parameter that is predicted according to Eq. 29 is $B_{m^*\zeta}$ =0.01311.

4.3.2.4 Frequency Ratio (Reduced Frequency) f^*

The frequency ratio f^* can be defined as:

$$f^* = \frac{f_{osc}}{f_{n,w}} \tag{30}$$

where f_{osc} is frequency of oscillation of the cylinder and $f_{n,w}$ is natural frequency in water. Natural frequency of the system, given by Eq. 31 is the main component of examining the vortex-induced vibration phenomenon (Modir and Goudarzi, 2019).

$$f_{n,w} = \frac{1}{2\pi}\sqrt{\frac{K}{m_{osc}+m_a}} \tag{31}$$

where K is spring stiffness, m_{osc} is oscillating mass and m_a is ideal added mass.

The added mass can be formulate as

$$m_a = C_a\, m_{disp}$$

C_a=1 for a circular cylinder. Thus, in VIV tests that is used cylinder $m_a = m_d$. So the Eq. 34 turns to Eq. 32.

$$f_{n,w} = \frac{1}{2\pi}\sqrt{\frac{K}{m_{osc}+\pi/4\,\rho\, D^2\, L}} \tag{32}$$

The mathematical definition and the bias uncertainty of the frequency ratio f^* are given by Eq. 33 and Eq. 34, respectively.

The total bias uncertainty for the frequency ratio f^*), calculated according to Eq. 34 is $B_{f^*} = 0.0064$.

$$f^* = \frac{f_{osc}}{f_{n,w}} = \frac{f_{osc}}{\frac{1}{2\pi}\left(\frac{K}{m_{osc}+\pi/4\,\rho\, D^2\, L}\right)^{1/2}} = f_{osc}\, 2\pi \left(\frac{m_{osc}+\pi/4\,\rho\, D^2\, L}{K}\right)^{1/2} \tag{33}$$

$$B_{f^*} = \sqrt{\left(\frac{\partial f^*}{\partial L} B_L\right)^2 + \left(\frac{\partial f^*}{\partial D} B_D\right)^2 + \left(\frac{\partial f^*}{\partial \rho} B_\rho\right)^2 + \left(\frac{\partial f^*}{\partial m_{osc}} B_{m_{osc}}\right)^2 + \left(\frac{\partial f^*}{\partial K} B_K\right)^2 + \left(\frac{\partial f^*}{\partial f_{osc}} B_{f_{osc}}\right)^2} \tag{34}$$

4.3.2.5 Reduced Velocity U^*

The non-dimensional parameter that indicates the vibration amplitude is the reduced velocity U^*. Mathematical definition of reduced velocity is given by Eq. 35:

$$U^* = \frac{U}{f_{n,w}\, D} \tag{35}$$

In order to calculate the bias error for the reduced velocity, first it is needed to calculate the bias error of the natural frequency in water. Mathematical definition of the reduced velocity utilized in this study is given by Eq. 36.

$$U^* = 2\pi\, U \left(\frac{m_{osc}+\pi/4\,\rho\, D^2\, L}{D^2\, K}\right)^{1/2} \tag{36}$$

The bias uncertainty of the reduced velocity (U^*) is calculated as given by Eq. 37 below.

The total bias uncertainty for the reduced velocity calculated according to Eq. 37 is $B_{U^*} = 0.00906$

4.3.2.6 The phase Angle (Φ)

The phase angle (Φ) represents the phase difference of the fluid force and the displacement. Bias error for

the phase angle Φ) is supposed as B_Φ= 0.010 in the bias uncertainty calculations.

4.3.2.7 Added Mass Coefficient (C_A)

The added mass coefficient C_A =1.0 for a circular cylinder (Modir and Goudarzi, 2019). For this reason, it is not necessary to calculate the bias error for the C_A.

4.3.3 Total Bias Uncertainty for the Flow Velocity U=0.338 m/s

Bias errors obtained from the above calculations are given in Table 3.

Total bias uncertainty of response amplitude B_{A^*} is calculated by using Eq. 38 as B_{A^*}=0.0199.

$$U^* = \sqrt{\left(\frac{\partial U^*}{\partial L}B_L\right)^2 + \left(\frac{\partial U^*}{\partial D}B_D\right)^2 + \left(\frac{\partial f^*}{\partial \rho}B_\rho\right)^2 + \left(\frac{\partial f^*}{\partial m_{osc}}B_{m_{osc}}\right)^2 + \left(\frac{\partial f^*}{\partial K}B_K\right)^2 \left(\frac{\partial f^*}{\partial U}B_U\right)^2} \quad (37)$$

$$B_{A^*} = \sqrt{\left(B_{C_y}\right)^2 + (B_{m^*})^2 + \left(B_{m^*\zeta}\right)^2 + \left(B_{f^*}\right)^2 + (B_{U^*})^2 + (B_\Phi)^2} \quad (38)$$

Table 3 Bias uncertainty components for U=0.338 m/s

Uncertainty source	Calculated B Errors
Lift coefficient B_{C_y}	0.0588
Mass ratio B_{m^*}	0.0085
Mass-damping parameter B_m	0.0131
Frequency ratio B_{f^*}	0.0064
Reduced velocity B_{U^*}	0.0090
The phase angle B_Φ	0.010

This error corresponds to the 2.123 % of the mean A^* value of 0.937.

4.4 Uncertainty Analysis for VIV Tests in Flow Velocity U=0.390 m/s and U=0.442

Uncertainty analysis are repeated for two more distinct flow velocities, U=0.390 m/s and U=0.442 m/s, using the same procedure given in Sections 4, up to this sub-section.

4.4.1 Uncertainty Analysis for VIV Tests in Flow Velocity U=0.390 m/s

While calculating the precision error, test measurements of 5 sets of VIV tests at the flow velocities of U= 0.390 m/s are used. As a result, of 5 repetitions of the experiments, mean values and standard deviations are calculated given in Table 4.

Table 4 Precision uncertainty data for U=0.390 m/s

Test No	Measured Values		
	A^*	f^*	C_y
1	0.7482	1.0177	0.3493
2	0.8267	1.0115	0.3836
3	0.7763	1.0115	0.3602
4	0.7597	1.0207	0.3558
5	0.8275	1.0133	0.3846
Mean	0.7877		0.3667
Sdev			0.0146

Table 5 Bias uncertainty components for U=0.390 m/s

Uncertainty source	Calculated Bias Errors
Lift coefficient B_{C_y}	0.0065
Mass ratio B_{m^*}	0.0085
Mass-damping parameter B_{π}	0.0132
Frequency ratio B_{f^*}	0.0064
Reduced velocity B_{U^*}	0.0090
The phase angle B_Φ	0.010

Total precision uncertainty of response amplitude is predicted using Eq. 9 as P_{A^*}= 0.0293.

This error corresponds to the 3.717 % of the mean A^* value of 0.7877.

Bias errors for response amplitude value, obtained from the predictions for U= 0.390 m/s are given in Table 5.

Total bias uncertainty of response amplitude B_{A^*} can be calculated by the Eq. 38.

$$\sqrt{\left(B_{C_y}\right)^2 + (B_{m^*})^2 + \left(B_{m^*\zeta}\right)^2 + \left(B_{f^*}\right)^2 + (B_{U^*})^2 + (B_\Phi)^2}$$

For Flow velocity U=0.390 m/s; B_{A^*} = 0.0211.

This uncertainty corresponds to the 2.678 % of the mean A^* value of 0.7877.

4.4.2 Uncertainty Analysis for VIV Tests in Flow Velocity U=0.442 m/s

While calculating the precision error, test measurements of 5 sets of VIV tests at the flow velocities of U= 0.442 m/s presented in Table 6 are used.

Total precision uncertainty of response amplitude is predicted using Eq. 9 as P_{A^*}= 0.0181.

This error corresponds to the 2.636 % of the mean A^* value of 0.6861.

Bias errors obtained from the calculations for U= 0.442 m/s are given in Table 7.

Total bias uncertainty of response amplitude B_{A^*} can be calculated by the Eq. 38.

Table 6 Precision uncertainty data for U=0.442m/s

Test No	Measured Values		
	A^*	f^*	C_y
1	0.6604	1.1114	0.2621
2	0.6706	1.1180	0.2678
3	0.7197	1.1142	0.2864
4	0.6731	1.1161	0.2683
5	0.7066	1.1127	0.2808
Mean	0.6861		0.273100
Sdev			0.009043

Table 7 Bias uncertainty components for U=0.442 m/s

Uncertainty source	Calculated Bias Errors
Lift coefficient B_{C_y}	0.0106
Mass ratio B_{m^*}	0.0085
Mass-damping parameter B_{π}	0.0131
Frequency ratio B_{f^*}	0.0072
Reduced velocity B_{U^*}	0.0118
The phase angle B_{Φ}	0.010

$$\sqrt{\left(B_{C_y}\right)^2 + (B_{m^*})^2 + \left(B_{m^*\zeta}\right)^2 + \left(B_{f^*}\right)^2 + (B_{U^*})^2 + (B_{\Phi})^2}$$

B_{A^*} = 0.0235.

This error corresponds to the 3.428 % of the mean A^* value of 0.6861.

4.5 Uncertainty Analysis Results of VIV Tests and Discussions

Bias (systematic) error depends on the uncertainties of basic parameters such as model length, model diameter, displacement of cylinder, density of water, temperature of water, flow velocity and kinematic viscosity of water.

The amplitude of a cylinder in VIV tests, however, mainly depends on the components, which are given in Eq. 7, such as the magnitude of the force coefficients, mass ratio (the relative mass of the body to the displaced water mass), flow velocity (reduced velocity), structural damping and the parameters related frequency of vibration. Accordingly, it would be reasonable to calculate the uncertainty level using these parameters. Within this context, the bias error components for VIV tests may be sorted as lift coefficient, mass ratio, mass-damping parameter, frequency ratio, reduced velocity and phase angle.

Precision uncertainty is evaluated via repeated measurements. 5 sets of measurements for different flow velocities provide sufficient data for the standard deviation to include random errors. In the light of these components of uncertainty tests, uncertainty levels for the response amplitude values obtained by VIV tests conducted at Ata Nutku Laboratory are tabulated in Table 8.

Table 8 Uncertainty results of the VIV tests at Ata Nutku Laboratory of ITU (% of A^*)

U (m/s)	Bias uncertainty (% of A^*)	Precision Uncertainty (% of A^*)	Total uncertainty (% of A^*)
U=0.338	2.123	2.393	3.199
U=0.380	2.678	3.717	4.581
U=0.442	3.428	2.636	4.324

Considering the results presented in Table 8, it can be point out that, the total uncertainty of the VIV tests for the selected flow velocities in this study are in the range of 3-5%. This means that the VIV tests were carried out with the 95% confidence level. In other words, the tests have low uncertainty. Besides, the total bias and precision uncertainties are quite close to each other.

These results show the reliability a of the VIV tests conducted at the circulation channel of Ata Nutku Laboratory in Istanbul Technical University.

5. CONCLUSIONS

In this study, uncertainty analysis of the vortex-induced vibration (VIV) tests carried out on the circulation channel in Ata Nutku Ship Model Testing Laboratory at Istanbul Technical University (ITU). Five distinct VIV tests, following ITTC recommended guidelines, have been performed using similar parameters and under same conditions in order to observe the effects of the uncertainty involved in experiments. The amplitude (A^*) and frequency (f^*) data are obtained from VIV tests and uncertainty analysis study is performed for three different flow velocities. Bias and precision uncertainties are predicted, using the components of the amplitude response (A^*) values for the cylinder and total uncertainties for different flow velocities are presented. Based on the test results and uncertainty analysis, following conclusions are drawn:

- Currently, ITTC does not propose a clear VIV uncertainty methodology and studies based on calculation of uncertainty levels of ITTC tests are limited. In this study, a procedure normally used in different disciplines, such as ship resistance and propulsion tests, are applied and is expected to provide an example to predict the uncertainty for VIV tests.
- The test results have demonstrated that the VIV test rig that is used has low uncertainty level. Additionally, it has succeeded to reflect the characterictics of VIV phenomenon in the studied Reynolds number range, which is in the transition in shear layer 3 (TrSL3) flow regime.
- The proposed procedure, that is based on the ASME method is a reliable and repeatable approach for uncertainty analysis of VIV tests. To the authors' knowledge, uncertainty components, bias and precision uncertainties of VIV tests are predicted for the first time in the literature in this study.

The VIV test results, utilized in this study are obtained using the VIV test rig that is installed on the circulation channel of Ata Nutku Ship Model Testing Laboratory located in Istanbul Technical University. The components of the VIV test rig is planned to be introduced in detail in the future.

Further future studies are expected to cover numerical uncertainties involved in CFD simulations.

REFERENCES

AIAA S-071A (1999). Assessment of experimental uncertainty with application to wind tunnel testing. *American Institute of Aeronautics and Astronautics*, Reston, Virginia, USA.

Arshad, H., S. Khushnood, L. Ahmad Nizam, M. Ameer Ahsan and O. Ghufran Bhatti (2018). Effect of fin geometry on flow-induced vibration response of a finned tube in a tube bundle. *Journal of Applied Fluid Mechanics* 11(4), 1143-1152.

ASME, PTC (2005). Test Uncertainty, *19. American Society of Mechanical Engineers*, New York, USA.

Bernitsas, M. M., J. Ofuegbe, J. U. Chen and H. Sun (2019). Eigen-solution for flow induced oscillations (VIV and Galloping) revealed at the fluid-structure interface. *38th International Conference on Ocean, ASME 2019, Offshore and Arctic Engineering*, American Society of Mechanical Engineers Digital Collection.

Bernitsas, M. M., K. Raghavan, Y. Ben-Simon and E. M. Garcia (2008). VIVACE (Vortex Induced Vibration Aquatic Clean Energy): A new concept in generation of clean and renewable energy from fluid flow. *Journal of Offshore Mechanics and Arctic Engineering* 130(4), 041101.

Bunt, E. V. D., J. Dekker, J. Tukker and M. V. Rijsbergen (2019). Levels for the evaluation of uncertainty in hydrodynamic model testing. AMT'19, *The Sixth International Conference on Advanced Model Measurement Technology for The Maritime Industry*, 9-11 October 2019, Rome Italy.

Carberry, J. (2001). *Wake States of a Submerged Oscillating Cylinder and of a Cylinder Beneath a Free Surface*. PHD Thesis, Monash University, Australia.

Delen, C. and S. Bal (2015). Uncertainty analysis of resistance tests in Ata Nutku Ship Model Testing Laboratory of Istanbul Technical University. *Turkish Journal of Maritime and Marine Sciences* 1(2), 69-88.

Dobrucali, E. and O. K. Kinaci (2017). URANS-based prediction of vortex induced vibrations of circular cylinders. *Journal of Applied Fluid Mechanics 10(3), 957-970.*

Duranay, A and O. K. Kinaci (2020). Enhancing two-dimensional computational approach for vortex-induced vibrations by scaling lift force. Ocean Engineering, 217, 107620.

Gopalkrishnan, R. (1993). *Vortex Induced Forces on Oscillating Bluff Cylinders*, Ph.D. Thesis. Department of Ocean Engineering, MIT.

Grioni, M., S. A. Elaskar and A. E. Mirasso (2020). A numerical study of the flow interference between two circular cylinders in tandem by scale-adaptive simulation model. *Journal of Applied Fluid Mechanics* 13(1), 169-183.

Insel, M. (2008). Uncertainty in the analysis of speed and powering trials, *Ocean Engineering* 35, 1183–1193.

ISO (2008) Uncertainty of Measurement, Part 3: Guide to the Expression of Uncertainty in Measurement, *GUM: 1995*, ISO guide 98-3.

ITTC, Report No 7.5-01-01-01 (2002). Recommended Procedures and Guidelines, *Model Manufacture Ship Models.*

ITTC, Report No 7.5-02-01-01 (2014). Recommended Procedures and Guidelines, *Guide to the Expression of Uncertainty in Experimental Hydrodynamics*.

ITTC, Report No 7.5-02-02-02 (2002). Recommended Procedures and Guidelines. *Testing and Extrapolation Methods Resistance Uncertainty Analysis, Example for Resistance Test.*

ITTC, Report No 7.5-02-02-02 (2014). Recommended Procedures, *General Guideline for Uncertainty Analysis in Resistance Tests*.

ITTC, Report No 7.5-02-03-01.2 (2017). Recommended Procedures and Guidelines, *ITTC Quality System Manual Recommended Procedures and Guidelines, Uncertainty Analysis, Example for Propulsion Test.*

ITTC, Report No 7.5-02-07-03.10 (2014). Recommended Procedures and Guidelines, Guideline for VIV Testing, *ITTC Quality System Manual Recommended Procedures and Guidelines, Guideline for VIV Testing*.

ITTC, Report No, 7.5-02 01-03 (1999). Recommended Procedures, Testing and Extrapolation Methods, *General Density and Viscosity of Water*.

JCGM 100:2008 (2008). GUM 1995 with minor corrections, *Evaluation of measurement data - Guide to the expression of uncertainty in measurement.*

Khalak, A. and C. H. K. Williamson (1999). Motions, Forces and Mode Transitions in Vortex-Induced Vibrations at Low Mass-Damping. *Journal of Fluids and Structures* 13, 813–851.

Kinaci, O. K. (2016). 2-D URANS Simulations of Vortex Induced Vibrations of Circular Cylinder at TrSL3 Flow Regime. *Journal of Applied Fluid Mechanics* 9(5), 2537-2544.

Kinaci, O. K., S. Lakka, H. Sun and M. M. Bernitsas

(2016a). Effect of tip-flow on vortex induced vibration of circular cylinders for Re<1.2* 10^5. *Ocean Engineering* 117, 130-142.

Kinaci, O. K., S. Lakka, H. Sun, E. Fassezke and M. M. Bernitsas, (2016b). Computational and experimental assessment of turbulence stimulation on flow induced motion of a circular cylinder. *Journal of Offshore Mechanics and Arctic Engineering* 138(4).

Klamo, J. T., A. Leonard and A. Roshko (2005). On the Maximum Amplitude for a Freely Vibrating Cylinder in Cross-Flow, *Journal of Fluids and Structures* 21, 429–434.

Lee, J. H. and M. M. Bernitsas (2011). High-damping, high-Reynolds VIV tests for energy harnessing using the VIVACE converter, *Ocean Engineering* 38 (16), 1697-1712.

Modir A., M. Kahrom and A. Farshidianfar (2016). Mass ratio effect on vortex induced vibration of a flexibly mounted circular cylinder, an experimental study, *International Journal of Marine Energy* 16, 1–11.

Modir, A. and N. Goudarzi (2019). Experimental investigation of Reynolds number and spring stiffness effects on vortex induced vibrations of a rigid circular cylinder. *European Journal of Mechanics / B Fluids 74, 34–40.*

Mumtaz Qadri, M. N., A. Shahzad, F. Zhao and H. Tang (2019). An experimental investigation of a passively flapping foil in energy harvesting mode. *Journal of Applied Fluid Mechanics* 12(5), 1547-1561.

Park, D. M., J. Lee and Y. Kim (2015). Uncertainty analysis for added resistance experiment of KVLCC2 ship. *Ocean Engineering* 95, 143–156.

Pigazzini, R., G. Contento, S. Martini, T. Puzzer, M. Morgut and A. Mola (2018). VIV analysis of a single elastically-mounted 2D cylinder: Parameter identification of a single-degree-of-freedom multi-frequency model. *Journal of Fluids and Structures* 78, 299-313.

Qiu, W. (2014). *Report of the Ocean Engineering Committee,* 28th ITTC, Copenhagen, Denmark.

Qui, W., J. S. Junior, D. Lee, H. Lie, V. Magarovskii, T. Mikami, J. M. Rousset, S. Sphaier, L. Tao and X. Wang (2014). Uncertainties related to predictions of loads and responses for ocean and offshore structures. *Ocean Engineeering* 86, 58-67.

Raghavan, K. and M. M. Bernitsas (2011). Experimental investigation of Reynolds number effect on vortex induced vibration of rigid circular cylinder on elastic supports. *Ocean Engineering* 38(5-6), 719-731.

Sarpkaya, T (2004). A critical review of the intrinsic nature of vortex induced vibrations. *J. Fluids Struct.* 19 (4), 389–447.

Sumer, B. M. and J. Fredsoe (2006). Hydrodynamics around cylindrical structures. *Advanced Series on Ocean Engineering,* 26.

Tezdogan, T, Demirel, Y. K., Kellett, P., Khorasanchi, M., Incecik, A. and O. Turan. Full-scale unsteady RANS CFD simulations of ship behavior and performance in head seas due to slow steaming. *Ocean Engineering* 97, 186-206.

Usta, O. and E. Korkut, Korkut (2018). A study for cavitating flow analysis using DES model. *Ocean Engineering* 160, 397–411.

Williamson, C. H. K. and R. Govardhan (2004). Vortex induced vibrations. *Annual Review of Fluid Mechanics* 36, 413–455.

Williamson, C. H. K. and R. Govardhan (2006). Defining the 'modified Griffin plot' in vortex-induced vibration: revealing the effect of Reynolds number using controlled damping. *Journal of Fluid Mechanics* 561, 147–180.

Wu, W., M. M. Bernitsas and K. Maki, (2014). RANS simulation versus experiments of flow induced motion of circular cylinder with passive turbulence control at 35,000<Re<130,000. *Journal of Offshore Mechanics and Arctic Engineering* 136(4).

Zhang, B., B. Song, Z. Mao, W. Tian and B. Li (2017). Numerical investigation on VIV energy harvesting of bluff bodies with different cross sections in tandem arrangement. *Energy* 133, 723-736.